# $TiO_2$-CNT´s-Cu thin films: photocatalytic applications in the visible region

G. Jiménez Bolaina[a], L. Rojas Blanco[a], F. Paraguay-Delgado[b],
E. M. López Alejandro[a], T. Gonzalez-Sanchez[a], R. Castillo-Palomera[a],
E. Ramírez Morales[a,*]
[a] *Juárez University of Tabasco, Avenida Universidad S/N, Col. Magisterial, Villahermosa, Tabasco. CP. 86040 México*
[b] *Center for Research in Advanced Materials, Av. Miguel de Cervantes Saavedra 120, Complejo Industrial Chihuahua, 31136 Chihuahua, Chihuahua, México*

$TiO_2$, $TiO_2$-Cu, $TiO_2$-CNTs y $TiO_2$-CNTs-Cu films were obtained by Dip-coating technique and 500°C for 1h. The Anatase phase of $TiO_2$ was identified and the $TiO_2$-Cu film also presented the Tenorite secondary phase of CuO. The planes (101) and (200) of the Graphite 2H phase were identified in the films with CNTs. The crystal size was obtained between 5 to 16 nm. The morphology is homogeneous without pores and without cracks. The bandgap value for $TiO_2$-CNTs-Cu and $TiO_2$ films were 3.22 and 3.48 eV respectively. For photocatalytic evaluation Visible and UV irradiation were used and $TiO_2$-CNTs showed a degradation of 53%.

(Received October 7, 2023; Accepted January 17, 2024)

*Keywords:* Sol-gel, Thin film, Dip-coating, Photocatalysis

## 1. Introduction

Currently, interest has increased in photocatalysis for the elimination of contaminants present in wastewater discharged into various effluents. Among the contaminants that affect the chemical composition of water (pH, loss of biodiversity) [1] are: heavy metals [2], aromatic compounds [3], pesticides [4], pharmaceutical products [5] and synthetic dyes [6]; which are mainly used in the food industry and the textile industry. At present, the interest in photocatalytic applications for the degradation of pollutants in water has increased due to the various industrial wastes that seriously affect the environment.

The dyes are also carcinogenic and toxic to fauna in direct contact with them [7]. One of the main disadvantages of using dyes is that it is a refractory molecule and does not degrade easily due to the aromatic structure of the molecule [8].

There are various wastewater treatment methods, such as membranes [9], adsorption [10], reverse osmosis [11], activated carbon filters [12], biological and oxidative methods, however their efficiency is limited by the energy required [13,14]; Furthermore, with some methods the contaminants are transformed into other species. Advanced Oxidation Processes (AOPs) allow the degradation of persistent and refractory organic pollutants, generating oxidative species such as -OH, -$SO_4^2$ and -Cl [15].

Photocatalysis is an economical, reliable, and sustainable process that take advantage of the solar energy and its interaction with an oxide semiconductor to produce the charge carriers and trigger oxidative reactions to break the organic molecules to its mineralization to $H_2O$ and $CO_2$ molecules as final products of the reaction [16]. However, photocatalysis using $TiO_2$ (band gap of 3.2 eV) has been reported to be inefficient. For this reason, recent studies focus on improving photocatalytic materials by increasing the absorption range to increase the charge transfer on the surface of the material and reduce the recombination of electron-hole pairs [17]. For this reason, $TiO_2$ has been doped with materials such as $VO_2$, $Cu^{+2}$ [18], CuO [19,20], CNTs/$TiO_2$ [21], and CNTs/$TiO_2$/Cu [22], $ZrO_2$ [23,24] etc.

* Corresponding author: eriking10@hotmail.com
https://doi.org/10.15251/DJNB.2024.191.141

Research for wastewater treatment requires materials such as Carbon Nanotubes, with good optical, mechanical and chemical properties, in addition to their high efficiency in the degradation of harmful organic species. The capacity of CNT-based materials has been studied for organic dyes such as methyl orange, aromatic compounds such as phenol, and other contaminants such as heavy metals and humic acid [25]. Studies reveal an improvement in photocatalysis by incorporating carbon nanotubes (CNTs) to $TiO_2$, since the separation of photogenerated electro-hole pairs is promoted [26] and increases the size of the area and the rate of redox reactions. However, the ability to separate electron-hole pairs depends on the quality of interfacial contact between $TiO_2$ and CNTs [21].

In this work, $TiO_2$-CNTs-Cu films are synthesized by sol gel methods. In order to evaluate the effect of carbon nanotubes and Cu on the structure of TiO2. The aim is to introduce impurities to generate donor and acceptor species that allow taking advantage of the visible part of the solar spectrum and increasing the surface area.

## 2. Experimental

### 2.1. Synthesis

For the synthesis of the $TiO_2$ and impurified films, titanium tetrabutoxide (Aldrich), 2% by weight Copper Nitrate (Civeq) and 0.5% by weight CNT, were used. The solutions were made at room temperature and under stirring for 60 min.

### 2.2. $TiO_2$-CNTs-Cu thin films growth and annealing

For the deposit by the dip-coating method, 4 layers of $TiO_2$, $TiO_2$-CNTs, $TiO_2$-Cu and $TiO_2$-CNTs-Cu were made on Corning glass substrates with thicknesses of 222 nm, 245 nm, 434 nm and 328 nm respectively. To remove remaining solvents, each film was dried under air flow in an oven (XD-1200N) at 100°C for 5 minutes. For the crystallization of the films, a heat treatment was given at 500°C for 1 hr in air flow with a ramp of $10^oC$/min.

### 2.3. Photocatalytic degradation

For the photocatalytic activity, a Sciencetech SS0.5kW-1.6kW solar simulator and a tubular photoreactor with a 14 W T5 linear fluorescent UV irradiation lamp were used. The pollutant used was 1 ppm methylene blue. In the experiment, the films were immersed in the aqueous solution for 240 minutes, measuring the absorbance every 30 minutes.

### 2.4. Characterization

The transmittance of the films was evaluated with the Perking Elmer UV-VIS Lambda 9 model in the range from 200 to 1100 nm. Absorption spectra were performed with an Agilent 8453 Uv–Vis spectrophotometer with an interval of 190 – 1100 nm. The diffractograms were obtained with a Rigaku Ultima VI model diffractometer with Cu kα radiation (λ: 1.5418 Å), scan of 20-70°, rate of 1°/min and grazing beam of 1.0. The photoelectrochemical evaluation was performed with an AUTOLAB PGSTAT80N model galvanostat potentiostat with an applied voltage of 1 V for 300 seconds with intermittent lighting every 10 seconds using a 300 W OSRAM J338 halogen lamp (lamda=280 at 500 nm). TEM images were obtained with a Nanotech TEM Hitachi 7700 Transmission Electron Microscope. Raman spectra were obtained with a Micro Raman Horiba HR with a 635nm laser. The micrographs were obtained with a scanning electron microscope (SEM) model JSM 7401F.

## 3. Results and discussion

### 3.1. Characterization of thin films

The X-ray diffraction patterns of $TiO_2$, $TiO_2$-Cu, $TiO_2$-CNTs, $TiO_2$-CNTs and $TiO_2$-CNTs-Cu films are shown in Fig.1. The $TiO_2$ film shows the characteristic peaks of the anatase phase (PDF#21-1272) at angles 2θ: 25.36°, 37.9°, 48.1°, 54°, 55.2° and 62.86° corresponding to

the (1 0 1), (0 0 4), (2 0 0), (1 0 5), (2 1 1) and (2 0 4) planes [27]. According to the literature because there is a difference between the charge states of $Cu^{2+}$ and $Ti^{4+}$, oxygen vacancies are generated in the lattice structure of $TiO_2$ with Cu doping to maintain charge neutrality [18] However due to the low Cu concentration in the films it was not possible to identify any CuO phase as Tenorite (PDF#05-0661) (Fig. 1). On the other hand, the lattice parameters a, b and c was calculated using the equation $\frac{1}{d^2}\left(\frac{h^2+k^2}{a^2}+\frac{l^2}{c^2}\right)$(tetragonal), where $d_{hkl}$ is the spacing between adjacent lattice planes (hkl). An increase in lattice parameters was observed with the incorporation of Cu ($TiO_2$-Cu) with respect to $TiO_2$ (Anatase) film (Table 1), since the Cu precursor used is Copper Nitrate ($Cu(NO_3)_2$), there must be the presence of $Cu^{+2}$ ions in the solution. Comparing the ionic radii of $Cu^{+2}$ (0.69 Å) and $Ti^{+4}$ (0.68 Å), it is clear the possible substitution of $Ti^{+4}$ by $Cu^{+2}$ would be accompanied by a weak lattice expansion, due to the relatively small difference between their respective ionic radio [28, 29]. The films with CNTs showed an additional peak at 2θ=26.38 which corresponds to the (002) plane and is characteristic of the Graphite 2-H phase (PDF#41-1487). The crystal size was calculated using the equation of Debye–Scherrer $D=\frac{\kappa\lambda}{\beta cos\theta}$ , where D is the crystal size, the constant k=0.9, λ is the wavelength of the radiation, Θ is the diffraction angle and β is the broadening of diffraction lines measured as FWHM in radians. The calculated crystal size values were 17.9 nm for $TiO_2$ film, 14.89 nm with Cu and 12.29 with CNTs.

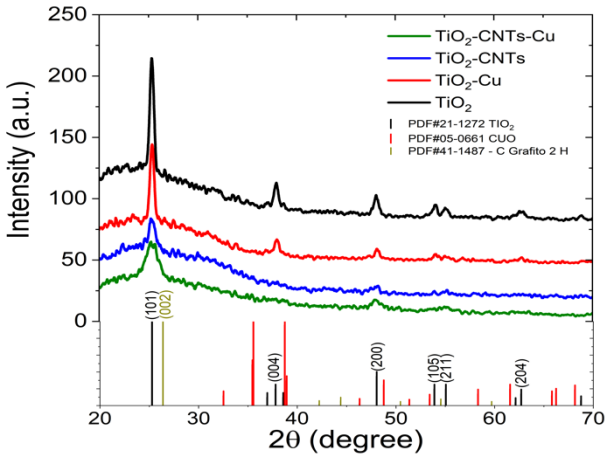


*Fig. 1. X-ray diffractograms of $TiO_2$, $TiO_2$-CNTs, $TiO_2$-Cu and $TiO_2$-CNTs-Cu thin films.*

*Table 1. Crystal size values and lattice parameters of $TiO_2$, $TiO_2$-CNTs, $TiO_2$-Cu and $TiO_2$-CNTs-Cu thin. films.*

| Sample | Lattice parameters (nm) | | Size cristal (nm) |
|---|---|---|---|
| | **a (Å)** | **c (Å)** | |
| $TiO_2$ | 3.776 | 9.486 | 17.9 |
| $TiO_2$.Cu | 3.7817 | 9.4714 | 14.89 |
| $TiO_2$.CNTs | 3.7842 | 9.4884 | 12.59 |
| $TiO_2$.CNTs-Cu | 3.7897 | 9.4944 | 12.59 |

In Fig.2(a) the transmittance spectra of the synthesized films are shown. It is observed that the transmittance decreases around 20% in the samples with CNT. According to the literature, these semiconductors are of indirect band [19, 20], which is related to the absorption coefficient and the energy of the incident photon by the Kubelka–Munk equation:

$$(\alpha hv) = A(hv - E_g)^n \quad (1)$$

where A is a constant, hv is the photon energy, α is the absorption coefficient obtained from the transmission coefficient T= exp(-α(ψ)d) [30], n is 1/2 (indirect allowed) and Eg is the energy gap. For the energy gap, the linear part of the graph $(\alpha\ hv)^{1/2}$ *vs* photon energy was extrapolated to the X axis. Bandgap values of 3.48 eV, 3.4 eV, 3.31 eV and 3.22 eV were obtained for $TiO_2$, $TiO_2$-Cu, $TiO_2$-CNTs and $TiO_2$-CNTs-Cu respectively (See Figure 2b and 2c). The band gap values are higher than those reported for $TiO_2$ anatase (3.0-3.2 eV), which is attributed to the grain size [31].

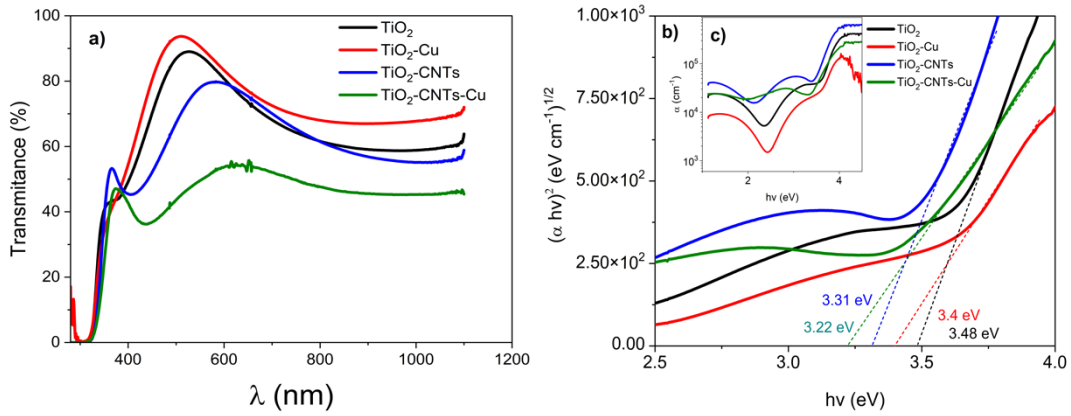


*Fig. 2. a) Transmittance spectra of $TiO_2$, $TiO_2$-Cu, $TiO_2$-CNTs and $TiO_2$-CNTs-Cu films, b) Linear fit for band gap calculation and c) Absorption coefficient graph.*

In the Raman spectra presented in Figure 3, vibrational modes reported for $TiO_2$ (anatase) are observed at: 144 $cm^{-1}$ (Eg), 197 $cm^{-1}$ (Eg), 399 $cm^{-1}$ (B1g), 513 $cm^{-1}$ (A1g), 519 $cm^{-1}$ (B1g) and 639 $cm^{-1}$ (Eg) [32]. In the spectrum with Cu, the CuO signal reported around 280 $cm^{-1}$ is not observed [33] . In the spectrum of the film with CNT a shift of the main vibrational mode towards the blue caused by an expansion of the anatase unit cell is observed [34]. Due to the low percentage of CNT used for the synthesis, the characteristic G and D lines of the tangential vibrations of the carbon atoms of the graphitic layers of the CNTs are not observed.

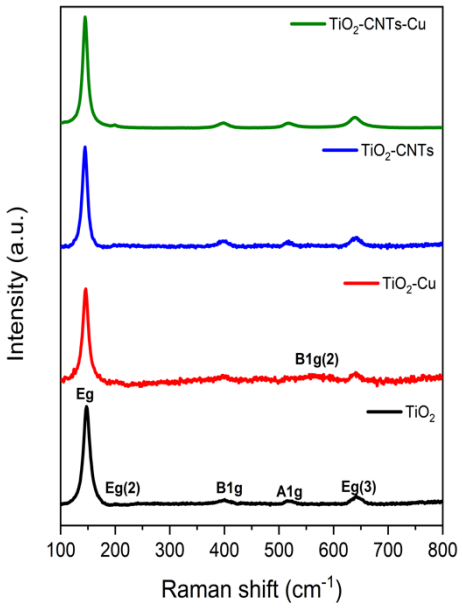


*Fig. 3. The vibrational modes in the Raman spectra of $TiO_2$, $TiO_2$-Cu, $TiO_2$-CNTs and $TiO_2$-CNTs-Cu.*

Figure 4 shows the selected area electron diffraction (SAED) patterns, in which the radio of the rings were measured and using the equation derived from Bragg's law and the diffraction geometry, the Interplanar distances were calculated with the following equation: $d = \frac{\lambda L}{r}$ ; Where r is the radius of the diffracted beam, λ is the wavelength of the electrons at the accelerating voltage used (100 kV= 0.037Å), L is the length of the chamber at which the microscope was used (30 cm). The Inter planar distances of the films are presented in Table 2. The $TiO_2$ film (Fig.4a) presented the crystallographic planes at (1 0 1), (1 0 3), (2 0 0), (1 0 5), (2 1 3) and (1 1 6) of the anatase phase of $TiO_2$ according to the crystallographic card (PDF#21-1272). All films exhibited the characteristic peaks of $TiO_2$ [35, 36]. The $TiO_2$-Cu sample (Fig.4b) presented an extra crystallographic plane at (-2 0 0) belonging to the CuO Tenorite crystalline phase (PDF#05-0661). This secondary phase was not possible to observe with XRD characterization [37]. The $TiO_2$-CNTs film (Fig.4c), showed the (101) and (200) planes respectively, from the crystallographic record PDF#41-1487 - C Graphite 2 H, in accordance with the analysis performed in XRD [38].

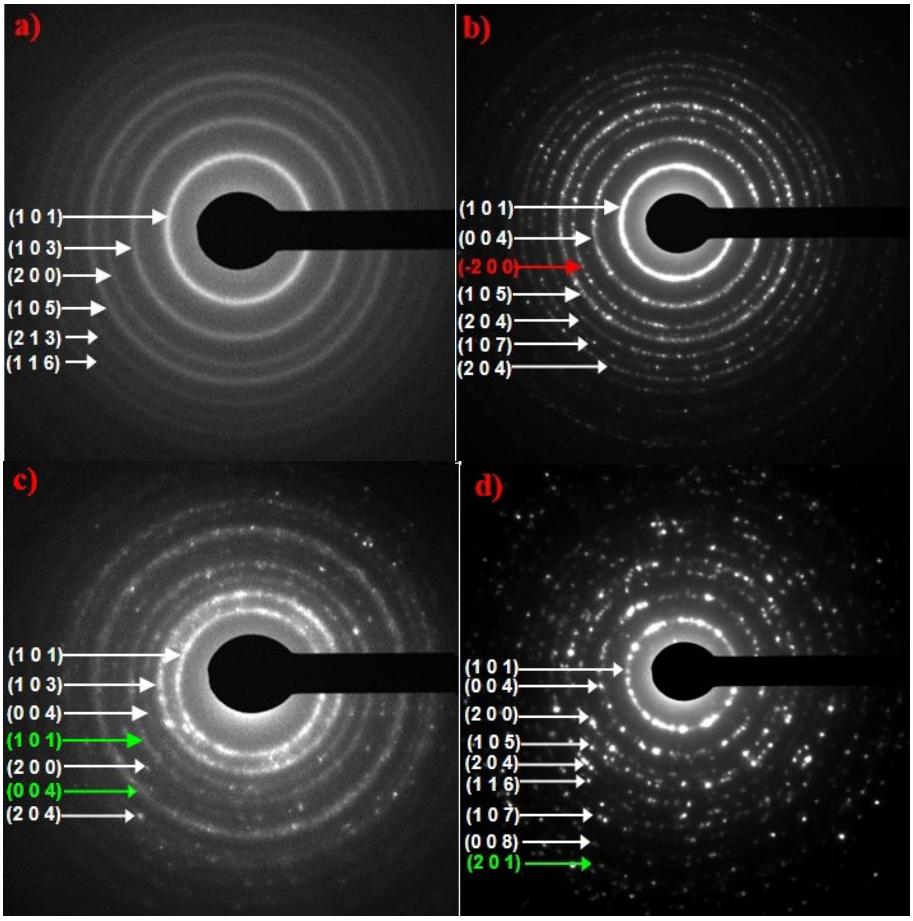


*Fig. 4. Electron diffraction pattern of a) $TiO_2$, b) $TiO_2$-Cu, c) $TiO_2$-CNTs and d) $TiO_2$-CNTs-Cu thin films.*

Figure 5 SEM surface micrographs of the $TiO_2$, $TiO_2$-Cu, $TiO_2$-CNTs and $TiO_2$-CNTs-Cu samples are presented. The $TiO_2$ film (Fig. 5a) shows a homogeneous morphology without clusters of material, non-porous and without cracks. The $TiO_2$-CNTs film shows a smooth surface, no cracks due to the different coefficients of thermal expansion with the Corning glass substrate. The $TiO_2$-CNTs-Cu film shows a homogeneous morphology without material clusters, non-porous and without visible cracks of the films.

*Table 2. Crystallographic interplanar film distances.*

| Lattice parameter (Å) | | | | |
|---|---|---|---|---|
| **(In this work)** | **PDF#21-1272 ($TiO_2$) Anatasa** | **PDF#41-1487 C Grafito 2 H** | **PDF#05-0661 (CuO) Tenorita** | **( h k l )** |
| **3.52** | 3.52 | | | **1 0 1** |
| **2.382** | 2.378 | | | **0 0 4** |
| **2.42** | 2.4243 | | | **1 0 3** |
| **1.897** | 1.892 | | | **2 0 0** |
| **1.859** | 1.888 | | 1.866 | **-2 0 0** |
| **1.708** | 1.6999 | | 1.714 | **1 0 5** |
| **1.490** | 1.493 | | | **2 1 3** |
| **1.484** | 1.4808 | | | **2 0 4** |
| **1.365** | 1.3641 | | | **1 1 6** |
| **1.280** | 1.280 | | | **1 0 7** |
| **1.181** | 1.1894 | | | **0 0 8** |
| **1.056** | 1.06 | 1.0567 | | **2 0 1** |

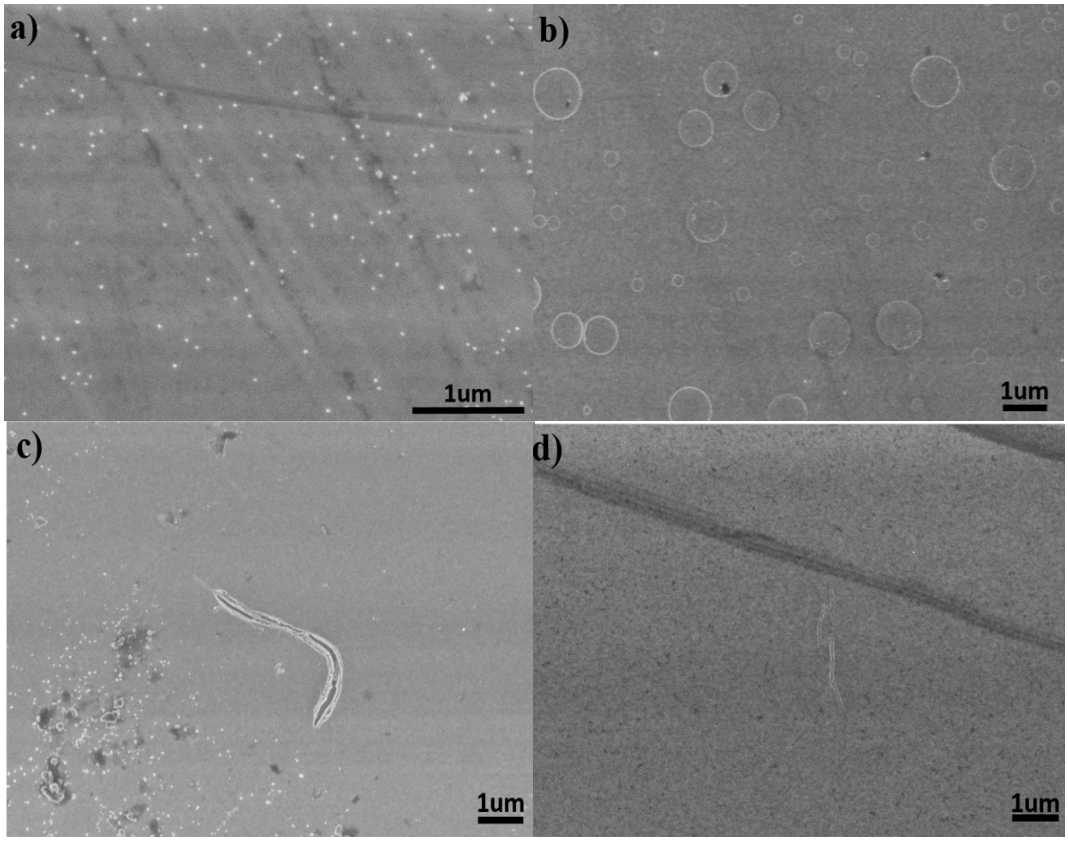


*Fig. 5. SEM micrographs of the thin films a) $TiO_2$, b) $TiO_2$-Cu, c) $TiO_2$-CNTs and d) $TiO_2$-CNTs-Cu.*

### 3.2 Photoelectrochemical evaluation

Figure 6 shows the chronoamperograms of the films. A 1 V positive potential for photoinduced electron-hole generation was applied by visible light irradiation for 10 sec and 10

sec in darkness over a surface area of 0.25 $cm^2$. The photosensitivity (S) of the samples was calculated using the following equation:

$$S = \frac{\sigma_i - \sigma_d}{\sigma_d} \quad (2)$$

where $\sigma_i$ and $\sigma_d$ are the conductivity in illumination and in darkness respectively. With the $TiO_2$ film, stability is observed with the presence and absence of light. The best value for the photosensitive response was 17.54 (See table 3). However, in the $TiO_2$-Cu film the current decreases, indicating instability in aqueous electrolytes [39]. Films with Cu showed a loss of photosensitivity, which can negatively affect photocatalytic activity.

*Table 3. Dark and illuminated conductivity values of $TiO_2$ thin films.*

| Sample | $\sigma_{dark}$ ($\Omega^{-1}cm^{-1}$) | $\sigma_{illumination}$ ($\Omega^{-1}cm^{-1}$) | Photosensitivity |
|---|---|---|---|
| **$TiO_2$** | $1.58 \times 10^{11}$ | $8.55 \times 10^{9}$ | 17.54 |
| **$TiO_2$-CNTs** | $6.94 \times 10^{10}$ | $4.15 \times 10^{9}$ | 15.73 |
| **$TiO_2$-Cu** | $1.46 \times 10^{10}$ | $9.80 \times 10^{9}$ | 0.55 |
| **$TiO_2$-CNTs-Cu** | $2.72 \times 10^{10}$ | 0 | 0 |

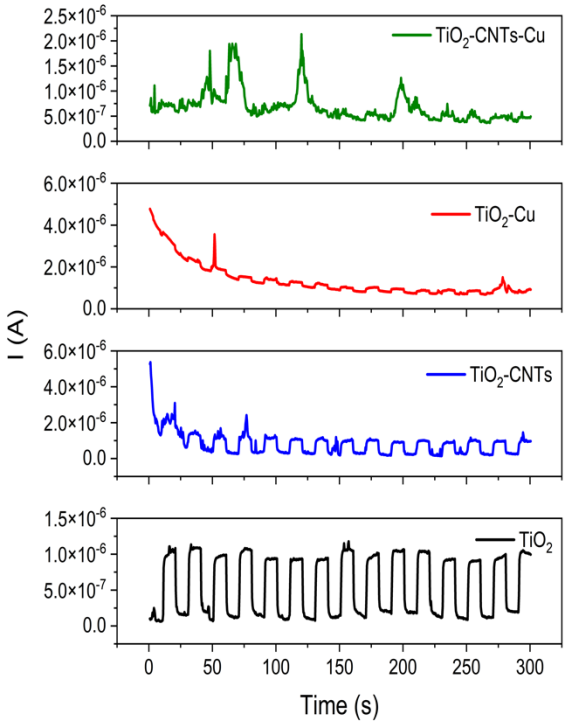


*Fig. 6. Chronoamperometry of the $TiO_2$, $TiO_2$-CNTs, $TiO_2$-Cu and $TiO_2$-CNTs-Cu samples.*

### 3.3. Characterization of Photocatalytic activity

Figure 7 shows the photocatalytic evaluation using UV light (Fig. 7a) and visible light (Fig.7b). As expected, the $TiO_2$ film showed photocatalytic efficiency only under UV light due to its 3.2 eV band gap. Films with carbon nanotubes exhibited higher photocatalytic activity, attributed to the photo-induced electron absorption effect of CNTs and the reduction of the electron-hole recombination rate on their surface [40]. The photocatalytic efficiencies of each film can be seen in Table 4.

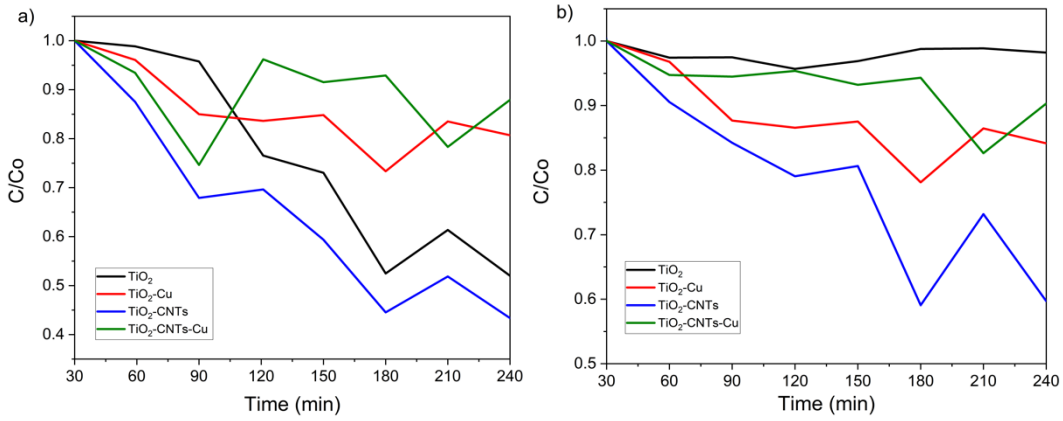


*Fig. 7. Photocatalytic efficiencies of methylene blue using $TiO_2$, $TiO_2$-Cu, $TiO_2$-CNTs and $TiO_2$-CNTs-Cu films under a) UV and b) Visible excitation*

*Table 4. Percentages of photocatalytic efficiency.*

| Sample | Fotodegradación de MB (%) | |
|---|---|---|
| | UV | Luz visible |
| $TiO_2$ | 44±5.2 | 3±1.2 |
| $TiO_2$-CNTs | 53±4.5 | 37±7.9 |
| $TiO_2$-Cu | 18±4.6 | 15±3.6 |
| $TiO_2$-CNTs-Cu | 16±6.8 | 8±4.8 |

## 4. Conclusions

$TiO_2$, $TiO_2$-Cu, $TiO_2$-CNTs and $TiO_2$-CNTs-Cu composites were successfully synthesized by the sol-gel technique and deposited as a thin film on a glass substrate by the Dip-coating method. The crystalline phase of the $TiO_2$ films was Anatase with a crystal size of 18 nm and a bandgap of 3.48 eV. The films doped with Cu showed a decrease in the network parameters, which is attributed to the substitution of Ti for Cu. The TEM results revealed the presence of the secondary phase of CuO (Tenorite), which is attributed to the decrease in the photoelectrolyte response and photocatalytic efficiency. On the other hand, with the $TiO_2$-CNTs film, a band gap shift from 3.48 eV (pure $TiO_2$) to 3.22 eV was obtained, and an improvement in conductivity and maximum photocatalytic degradation efficiency (53%) in a time of 190 min.

### Acknowledgements

G. Jiménez-Bolaina acknowledges CONACyT, Mexico, for financial support through the fellowship. L. Rojas-Blanco acknowledges a Consejo Estatal de Ciencia y Tecnología del Estado de Tabasco for the support with the project PRODECTI-2022-01/56

## References


[1] T. Islam, M.R. Repon, T. Islam, Z. Sarwar, M.M. Rahman, Environmental Science and Pollution Research. 30, 9207 (2023); https://doi.org/10.1007/s11356-022-24398-3

[2] X. Gao, X. Meng, Photocatalysis for heavy metal treatment: A review, Processes. 9, 1729 (2021); https://doi.org/10.3390/pr9101729

[3] R.M. Abdelhameed, M. El-Shahat, H.E. Emam, Carbohydr Polym. 247,116695 (2020); https://doi.org/10.1016/j.carbpol.2020.116695

[4] D. Vaya, P.K. Surolia, Environ Technol Innov 20, 101128 (2020); https://doi.org/10.1016/j.eti.2020.101128

[5] T. Velempini, E. Prabakaran, K. Pillay, Mater Today Chem. 19, 100380 (2021); https://doi.org/10.1016/j.mtchem.2020.100380

[6] R. Giovannetti, E. Rommozzi, M. Zannotti, C.A. D'Amato, Catalysts. 7, 305 (2017); https://doi.org/10.3390/catal7100305

[7] L.D. Ardila-Leal, R.A. Poutou-Piñales, A.M. Pedroza-Rodríguez, B.E. Quevedo-Hidalgo, Molecules. 26, 3813 (2021); https://doi.org/10.3390/molecules26133813

[8] Y. Wei, A. Ding, Y. Chen. J Environ Chem Eng. 10, 108524 (2022); https://doi.org/10.1016/j.jece.2022.10852

[9] S. Hube, M. Eskafi, K.F. Hrafnkelsdóttir, B. Bjarnadóttir, M.Á. Bjarnadóttir, S. Axelsdóttir, B. Wu, Science of the Total Environment. 710, 136375 (2020); https://doi.org/10.1016/j.scitotenv.2019.136375

[10] O.A. Adeleke, M.R. Saphira, Z. Daud, N. Ismail, A. Ahsan, N.A. Ab Aziz, A. Al-Gheethi, V. Kumar, A. Fadilat, N. Apandi, Nanotechnology in Water and Wastewater Treatment, Elsevier. 1 (2019); https://doi.org/10.1016/B978-0-12-813902-8.00001-0

[11] Y. Mikhak, M.M.A. Torabi, A. Fouladitajar, Sustainable Water and Wastewater Processing, Elsevier. 55 (2019); https://doi.org/10.1016/B978-0-12-816170-8.00003-X

[12] P.R. Dos Santos, L.A. Daniel, International Journal of Environmental Science and Technology. 17, 591 (2020); https://doi.org/10.1007/s13762-019-02567-1

[13] N. Dafale, N.N. Rao, S.U. Meshram, S.R. Wate, Bioresour Technol. 99, 2552 (2008); https://doi.org/10.1016/j.biortech.2007.04.044

[14] H. Han, M.K. Rafiq, T. Zhou, R. Xu, O. Mašek, X. Li, J Hazard Mater. 369, 780 (2019); https://doi.org/10.1016/j.jhazmat.2019.02.003

[15] D.B. Miklos, C. Remy, M. Jekel, K.G. Linden, J.E. Drewes, U. Hübner, Water Res. 139, 118 (2018); https://doi.org/10.1016/j.watres.2018.03.042

[16] M.E. Simonsen, Chemistry of Advanced Environmental Purification Processes of Water, Elsevier. 135–170 (2014); https://doi.org/10.1016/B978-0-444-53178-0.00004-3

[17] B.-Y. Wang, Y.-S. Hsiao, P.-C. Wei, Y.-T. Liu, C.-C. Chu, V.K.S. Hsiao, Catalysts 12, 564 (2022); https://doi.org/10.3390/catal12050564

[18] F. Bensouici, M. Bououdina, A.A. Dakhel, R. Tala-Ighil, M. Tounane, A. Iratni, T. Souier, S. Liu, W. Cai, Appl Surf Sci. 395, 110 (2017); https://doi.org/10.1016/j.apsusc.2016.07.034

[19] H. Koohestani, S.K. Sadrnezhaad, Desalination Water Treat. 57, 22029 (2016); https://doi.org/10.1080/19443994.2015.1132395

[20] M. Edelmannova, K.-Y. Lin, J.C.S. Wu, I. Troppova, L. Čapek, K. Kočí, Appl Surf Sci. 454, 313–318 (2018); https://doi.org/10.1016/j.apsusc.2018.05.123

[21] V. Rodríguez, R. Camarillo, F. Martínez, C. Jiménez, J. Rincón, J Supercrit Fluids. 163, 104876 (2020); https://doi.org/10.1016/j.supflu.2020.104876
[22] S.J. Hong, E.J.T. Pialago, H.H. Ha, O.K. Kwon, C.W. Park, Int J Heat Mass Transf. 157, 119935 (2020); https://doi.org/10.1016/j.ijheatmasstransfer.2020.119935
[23] K.Y. Jung, S. Bin Park, Mater Lett. 58, 2897 (2004); https://doi.org/10.1016/j.matlet.2004.05.015
[24] Y. Tao, S. Liu, T. Zheng, J. Lu, F. Li, R. Hao, H. Zhao, Z. Ma, L. Guo, Mater Lett. 311, 131589; https://doi.org/10.1016/j.matlet.2021.131589
[25] A.K. Haghi, K.M. Praveen, S. Thomas, AAP Research Notes on Nanoscience and Nanotechnology. (2016);
[26] Y. Wu, Z. Zhou, Y. Tuo, K. Wang, M. Huang, Y. Huang, S. Shen, Mater Chem Phys. 149, 522 (2015); https://doi.org/10.1016/j.matchemphys.2014.11.002
[27] Q. Qin, Q. Zhou, L.L. He, X.D. Zhu, W. Feng, J. Wang, Digest Journal of Nanomaterials & Biostructures (DJNB). 17 (2022); https://doi.org/10.15251/DJNB.2022.171.65
[28] M.C. Nevárez-Martínez, P.J. Espinoza-Montero, F.J. Quiroz-Chávez, B. Ohtani, Avances En Química. 12, 45 (2017);
[29] R.C. Zulkiflia, F. Azamanb, M.H. Razalia, A. Alib, M. Nora, Digest Journal of Nanomaterials & Biostructures (DJNB). 18 (2023); https://doi.org/10.15251/DJNB.2023.181.243
[30] S.R. Bhattacharyya, R.N. Gayen, R. Paul, A.K. Pal, Thin Solid Films. 517, 5530 (2009); https://doi.org/10.1016/j.tsf.2009.03.168
[31] Y. Mingmongkol, D.T.T. Trinh, D. Channei, W. Khanitchaidecha, A. Nakaruk, Mater Today Proc. 47, 3441 (2021); https://doi.org/10.1016/j.matpr.2021.03.330
[32] D. Komaraiah, E. Radha, J. James, N. Kalarikkal, J. Sivakumar, M.V.R. Reddy, R. Sayanna, J Lumin. 211, 320 (2019); https://doi.org/10.1016/j.surfin.2019.100368
[33] B. Shruthi, B.J. Madhu, V.B. Raju, S. Vynatheya, B.V. Devi, G. V Jayashree, C.R. Ravikumar, Journal of Science: Advanced Materials and Devices. 2, 93 (2017); https://doi.org/10.1016/j.jsamd.2016.12.002
[34] D. Komaraiah, E. Radha, J. Sivakumar, M.V.R. Reddy, R. Sayanna, Surfaces and Interfaces. 17, 100368 (2019); https://doi.org/10.1016/j.jlumin.2019.03.050
[35] E. Filippo, C. Carlucci, A.L. Capodilupo, P. Perulli, F. Conciauro, G.A. Corrente, G. Gigli, G. Ciccarella, Materials Research. 18, 473 (2015); https://doi.org/10.1590/1516-1439.301914
[36] S.E. Arasi, J. Madhavan, M.V. Antony Raj, Journal of Taibah University for Science. 12, 186 (2018); https://doi.org/10.1080/16583655.2018.1451057
[37] S. Toumi, A. Adawy, C. Marcos, Boletín de La Sociedad Española de Cerámica y Vidrio. (2023); https://doi.org/10.1016/j.bsecv.2023.08.001
[38] D. Dominguez, J.M. Romo-Herrera, F. Solorio, H.A. Borbón-Núñez, M. Landeros, J.N. Díaz de León, E. Contreras, O.E. Contreras, A. Olivas, E.A. Reynoso-Soto, Journal of Nanoparticle Research. 20, 1 (2018); https://doi.org/10.1007/s11051-018-4348-6
[39] S.T. Guerra, U.G. Sánchez, M.A.V. Zapata, Gen. 521, 140 (2016).
[40] M.A. Rodríguez-Meza, J.L. Cervantes-Cota, CIENCIA Ergo-Sum, Revista Científica Multidisciplinaria de Prospectiva. 13, 303 (2006).